Available online at www.sciencedirect.com
ScienceDirect
Journal of Photochemistry and Photobiology A: Chemistry 186 (2007) 158–165
Journal of Photochemistry and Photobiology A:Chemistry
www.elsevier.com/locate/jphotochem

Dynamics of photogenerated charge carrier and morphology dependence in polythiophene films studied by in situ time-resolved microwave conductivity and transient absorption spectroscopy

Akinori Saeki *, Shu Seki, Yoshiko Koizumi, Seiichi Tagawa *

The Institute of Scientific and Industrial Research, Osaka University, 8-1 Mihogaoka, Ibaraki, Osaka 567-0047, Japan

Received 31 March 2006; received in revised form 27 July 2006; accepted 12 August 2006
Available online 22 August 2006

Abstract

For the investigation of photoconductivity and charge carrier dynamics in regioregular poly(3-hexylthiophene) (RR-P3HT), an in situ flash-photolysis time-resolved microwave conductivity (FP-TRMC) and transient absorption spectroscopy (TAS) was performed using 6.4 and 3.5 eV photon excitation. Since the former energy is sufficiently higher than ionization potential of RR-P3HT, a direct ionization and consequent bulk charge recombination was observed. The dynamics of charge carriers of transient conductivity and photoabsorption kinetics are discussed in terms of the X-ray diffraction pattern and film morphology of RR-P3HT observed by tapping mode atomic force microscope.

Keywords: Microwave; Photoconductivity; Charge carriers; Polythiophene; Film morphology

1. Introduction

Optical, electrical and opto-electrical properties of π-conjugated polymers [1–3] have been investigated worldwide because of not only the scientific interests in the nature of charge carriers but also their feasibilities of functional devices such as flexible displays and thin film transistor. In order to reveal the dynamics and states of charge carriers, numerous investigations using magnetic spin resonance [4], transient/steady-state absorption/emission spectroscopies [5], and theoretical calculations [6] have been performed. A well-accepted model of charge state in general conjugated polymers is polaron and bipolaron which are localized charges on π-electron system coupling with the local chain geometry.

One of the reasons why conjugated polymers are expected in the use of flexible and low-cost transistor is their applicability to wet processing, due to their solubility for organic solvents. The solubility can be attained by substituting side chains for, e.g. alkyl groups. Among conjugated materials which show photo- and electro-luminescence, polythiophene and oligothiophene have been investigated as a typical π-conjugated material. The conductive property of polythiophene was considerably improved by the enhancement of regioregularity: the degree of head-to-tail–head-to-tail (HT–HT). Because of the increase of π-electron interaction, the high regioregularity yields well-organized π-stacking structures, leading to the formation of lamellar morphology [2].

As for the conductivity measurements, dc techniques such as time-of-flight and filed-effect-transistor have been used to date, in which the charge carriers are injected from polymer surface or attached electrodes into the polymer layer. In these experiments, the charge carriers travel over a long distance under a strong electric field, leading to a large contribution from impurities, domain boundary, pin hole, and so on.

On the other hand, time-resolve microwave conductivity (TRMC) [7] is a powerful tool for an electrodeless evaluation of conductivity. In TRMC method, charge carriers are generated by photo excitation or high energy radiation and probed by a low power microwave. Thus there is no need to attach an electrode, which leads to the elimination of effects of charge injection between the electrode and polymer layer. Using TRMC and 3 MeV electron beam, Grozema et al. [8] investigated charge carrier mobilities along isolated single polymer chain in solutions of various kinds of conjugated polymers, revealing that

* Corresponding authors. Tel.: +81 6 6879 8502; fax: +81 6 6876 3287.
E-mail addresses: saeki-a@sanken.osaka-u.ac.jp (A. Saeki), tagawa@sanken.osaka-u.ac.jp (S. Tagawa).

1010-6030/$ – see front matter © 2006 Elsevier B.V. All rights reserved.
doi:10.1016/j.jphotochem.2006.08.008

the intrinsic mobilities of charge carriers are several orders of magnitude higher than those obtained by dc technique. Dicker et al. [9] carried out TRMC experiments of regioregular polythiophene using a laser as an excitation source of which photon energy ranges from 1.9 to 5.2 eV and found the increasing quantum yield of photocarrier generation above 3.5 eV.

In this paper we report in situ TRMC and TAS (transient absorption spectroscopy) of regioregular poly(3-hexyl thiophene) (RR-P3HT) excited by 6.4 eV photon. Since this photon energy is much larger than the ionization potential, the conductivity signal is expected to increase, and therefore the dynamics of charge carriers changes with an increase in the density of charge carriers. The morphology of RR-P3HT solid films, namely the lamellar structure, would play an important role. We discuss the dependence of the morphology on the conductivity signal and kinetic traces of transient absorption, together with surface observations by atomic force microscope.

2. Experimental

Regioregular (head-to-tail >98%) poly(3-hexylthiophene) (RR-P3HT) was purchased from Aldrich, and used without further purification. Saturated *o*-dichlorobenzene or methyl tetrahydrofuran solution of RR-P3HT was drop-cast onto a quartz substrate (1 mm thick) and dried in a vacuum oven. The thicknesses of the films were measured by Dektak 3ST, giving ca. 0.5 μm for TRMC and TAS experiments and 3.5 μm for X-ray diffraction.

In situ time-resolved microwave conductivity (TRMC) and transient absorption spectroscopy (TAS) measurements of film samples was carried out using a X-band (ca. 9 GHz) microwave circuit, a nanosecond laser, and a streak camera. The power of the microwave incident into the cavity was set at 3 mW which does not disturb the charge motion and geminate ion recombination. The details of the measurement system will be reported elsewhere [10,11]. The THG (355 nm) from Nd:YAG laser (Spectra Physics, GCR-130, FWHM 5–8 ns) and ArF excimer laser (193 nm, Lambda Physik, Compex 102, FWHM 25–30 ns) were used as an excitation source. The spot size of the laser was adjusted at 4 mm diameter, and its power was set sufficiently low not to cause the ablation damages. Continuum white light from Xe lamp was used as a probe light and injected into the sample perpendicularly to the laser pulse. The spot size of the analyzing light was approximately 1 mm diameter at the sample. After passing through the sample, the white light continuum was led to a grating unit (Hamamatsu, C5094) and scanned by a wide-dynamic-range streak camera (Hamamatsu, C7700). The streak image was collected via a CCD camera (Hamamatsu, C4742-98). The experiments were carried out at room temperature and under the atmosphere.

The TRMC measurement with a resonant cavity is based on a microwave property that the change of reflected microwave power (ΔP_r) is proportional to the change of conductivity ($\langle\Delta\sigma\rangle$) induced by laser or radiation [11,12]:

$$\langle\Delta\sigma\rangle = \frac{1}{A}\frac{\Delta P_r}{P_r}, \tag{1}$$

where A is a sensitivity factor of a resonant cavity and is determined by a Q value, a dielectric constant, a resonant frequency, and a ratio of incident microwave power to reflected microwave power. In the case of flash-photolysis (FP)-TRMC, the following equation is obtained using Lambert–Beer's law:

$$\phi\sum\mu = \frac{1}{eAI_0F_{\text{Light}}}\frac{\Delta P_r}{P_r}, \tag{2}$$

where ϕ, $\Sigma\mu$, e, I_0, and F_{Light} are the quantum yield of charge carrier generation, the sum of charge carrier mobilities, the charge of an electron, incident photon density, and a correction (or filling) factor, respectively. The dimension of $\phi\Sigma\mu$ is the same as that of mobility ($\text{cm}^2\,\text{V}^{-1}\,\text{s}^{-1}$). The TRMC signals ($\Delta P_r/P_r$) are converted to $\phi\Sigma\mu$ by Eq. (2) in the present paper. The correction factor F_{Light} is calculated based on the optical property of the sample, intensity distribution of electric field in the resonant cavity [10,13], and the sample thickness.

The geometry of a sample set up is illustrated in Fig. 1(a), in which the half part of the resonant cavity is depicted. The

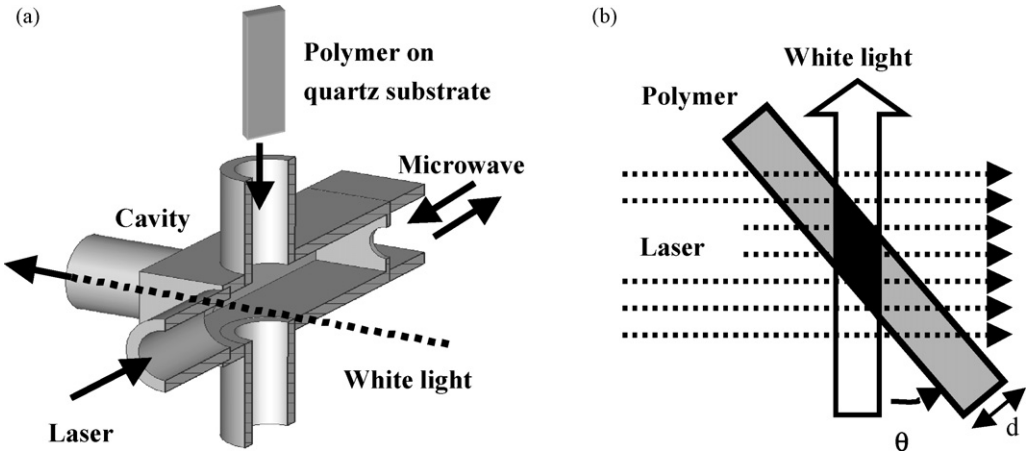

Fig. 1. Geometry of the sample loading part in in situ TRMC and TAS. (a) A half part of a resonant cavity for X-band (9 GHz) microwave is depicted with a polymer-casted quartz substrate, the incident directions of excitation laser, a probe light, and a microwave. (b) A schematic of a sample configuration viewed from the above. The sample is loaded inclining 45°.

use of the resonant cavity provides highly sensitive detection of changes in the conductivity. The resonant cavity used in the present system had five pipe windows. Two pipe windows at the top and the bottom of the cavity were used for sample loading, and another two on the side walls were opened as the path of analyzing light. The last one at the center of the end wall of the cavity was the entrance of the laser pulse. The electric field of this type of the cavity was simulated and used in the calculation of the correction factor [10]. In order to perform in situ TRMC and TAS measurements, a film sample is loaded inclining 45° as illustrated in Fig. 1(b).

In general, a coaxial optical geometry is used in optical spectroscopies. However, in the present system, a probe light is injected into the sample perpendicularly to the excitation laser for in situ experiments. The following expression gives the dependence of the transient optical density (O.D.) of the photo-induced transient species on the angle of a sample set up:

$$\frac{\text{O.D.}\,(\theta)}{\varepsilon\phi I_0} = \frac{1}{10N_\text{A}}\frac{1}{\tan\theta}(1-10^{-\alpha(d/\cos\theta)}), \tag{3}$$

where ε, N_A, θ, α, d are the extinction coefficient, Avogadro's number, the angle of a sample, the linear absorption coefficient, and sample thickness, respectively. Eq. (3) is limited in the case that a sample thickness is negligibly small compared with a spot size of a probe light. In addition, if θ is near 0 or 90°, Eq. (3) is not applicable, because the shape of probe area cannot be treated as parallelogram shown in Fig. 1(b). The inclined sample geometry undertakes Fresnel's formula given by

$$R_\text{s} = \left(\frac{n_2\cos\varphi - n_1\cos\theta}{n_2\cos\varphi + n_1\cos\theta}\right)^2, \tag{4}$$

$$R_\text{p} = \left(\frac{n_2\cos\theta - n_1\cos\varphi}{n_2\cos\theta + n_1\cos\varphi}\right)^2, \tag{5}$$

where R_s, R_p, n_1, n_2, θ, and φ are the reflectance of s-wave (TE mode), the reflectance of p-wave (TM mode), the refractive index of material 1, the refractive index of material 2, the angle of incidence, and the angle of reflection, respectively. In the present case, the materials 1 and 2 are an air and a polymer, respectively, and the laser pulse used is s-wave. The φ is expressed as a function of θ by the use of Snell's law:

$$\frac{\sin\varphi}{\sin\theta} = \frac{n_1}{n_2}. \tag{6}$$

By substituting $I_0(1-R_\text{s}(\theta))$ for I_0, Eq. (3) is transformed to the following expression:

$$\frac{\text{O.D.}\,(\theta)}{\varepsilon\phi I_0} = \frac{1}{10N_\text{A}}\frac{1}{\tan\theta}(1-10^{-\alpha(d/\cos\theta)})(1-R_\text{s}(\theta)). \tag{7}$$

If θ is equal to 0, namely a coaxial optical geometry, the left part of Eq. (7) is expressed by

$$\frac{\text{O.D.}_\text{coaxial}}{\varepsilon\phi I_0} = \frac{1}{10N_\text{A}}(1-10^{-\alpha d})(1-R_\text{s}(0)). \tag{8}$$

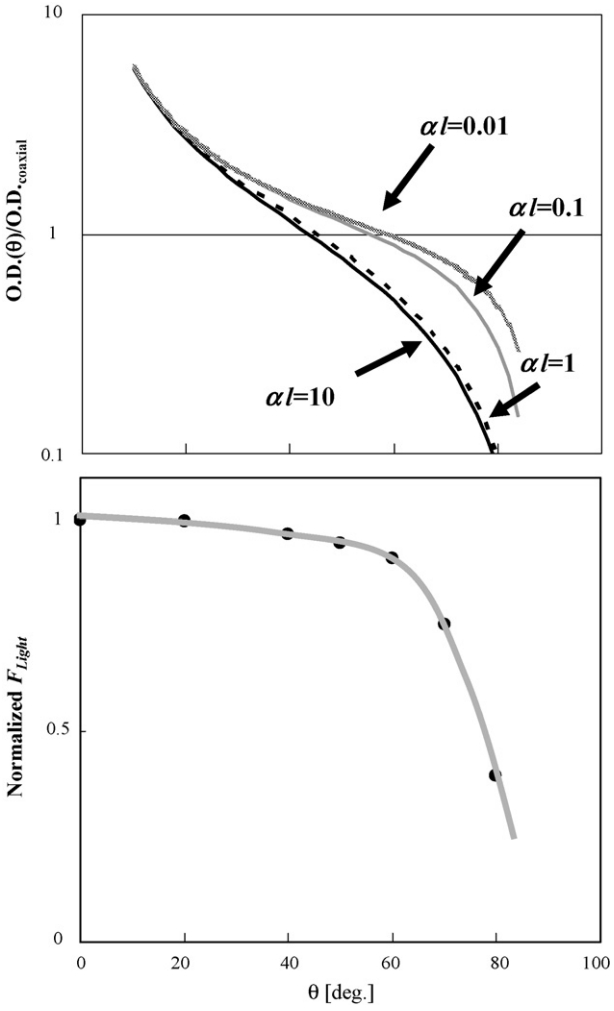

Fig. 2. Dependences of F_Light and O.D.(θ)/O.D.$_\text{coaxial}$ on the angle of sample (θ). The latter was calculated according to Eq. (9).

Therefore, the ratio of O.D.(θ) to O.D.$_\text{coaxial}$ is given by

$$\frac{\text{O.D.}\,(\theta)}{\text{O.D.}_\text{coaxial}} = \frac{1-10^{-\alpha(d/\cos\theta)}}{\tan\theta(1-10^{-\alpha d})}\frac{1-R_\text{s}(\theta)}{1-R_\text{s}(0)}. \tag{9}$$

Fig. 2(a) and (b) represents the dependences of F_Light and O.D.(θ)/O.D.$_\text{coaxial}$ on the angle of sample (θ), respectively. The $n_1 = 1$ (air) and $n_2 = 1.5$ (a typical value for polymers [14]) were used. If αl is more than 1, the O.D.(θ)/O.D.$_\text{coaxial}$ varies two orders of magnitude with the change of the sample angle, however, it is nearly equal to 1 at $\theta \sim 45°$. This means that the sensitivity of the optical spectroscopy is identical in both the coaxial and the 45° inclined geometries. The αl of the samples used in the present paper is more than 1, therefore any corrections are not necessary. The change of n_2 does not make significant difference in the range of $\alpha l > 1$. As can be seen from Fig. 2(a), the sensitivity is enhanced with the decrease of θ. However, the spectroscopies at such a small θ are difficult because of the decrease in the intensity of the probe light which can pass through a sample. As for F_Light shown in Fig. 2(b), it decreases with an increase of θ, but can be regarded as almost constant up to ~50°. Thus the inclined geometry at

$\theta = 45^\circ$ is the most appropriate for the in situ TRMC and TAS experiments.

The surface morphology of the polymer film was observed by a tapping mode atomic force microscope (AFM) (SPA-400, SEIKO Instruments Inc.). X-ray diffraction pattern was measured using Rigaku RU-200 (Cu Kα: 1.5418 Å, 50 kV, 150 mA).

3. Results and discussion

Transient absorption spectra of RR-P3HT film induced by 193 nm exposure is shown in Fig. 3. A broad absorption band and sharp bleaching maxima at 460 and 640 nm were observed. The bleaching of the steady-state absorption was observed fairly clear at the band edge of steady-state absorption. Thus the bleaching can be attributed to the positive charge on the longest π-conjugated segments after intra-molecular charge transfer from distributed length of the π-conjugated segments to the longest segments. The bleaching caused by one electron oxidation (positive polaron) of polymer chains was also measured by charge modulation spectroscopy (CMS) technique [15,16], in which the charges are injected into the polymer layer of FET-like device under modulated electric filed of about 200 kV/cm and transmitted probe light is detected. The bleaching maximum is centered at 2.21 eV (∼560 nm) with small peaks at 2.04 and 2.34 eV. These bleaching features fairly correspond to the vibronic structure of steady-state absorption spectra; however, the bleaching maximum observed in the present study is lying in the edge of steady-state absorption. This is due to the fact that the electric field of in situ TRMC measurement is approximately three orders of magnitude lower than that of CMS, leading to the charge migration to the longest π-conjugated segments without perturbing the motion of the charges. The charge transfer processes were, however, not observed because the processes occur within much faster time scale than the response time of the nanosecond TAS system. The kinetic traces at 460 and 640 nm in Fig. 3 are symmetrically identical over the entire time scale, suggesting that both the transient absorption and bleaching originate from one species: the positive charges on the longest π-conjugated segments.

Fig. 4 shows the TRMC (line) and TAS (closed circles) signals from RR-P3HT film excited by 193 nm pulses. The $\phi\Sigma\mu$ value is a product of quantum yield of charge carrier generation and the sum of positive and negative charge carrier mobilities. The kinetic traces of TAS were normalized to fit to those of TRMC in long time region. The photon energy of 193 nm is 6.4 eV which is higher than the reported ionization potential of polythiophene (∼5.4 eV) [17], so that the positive and negative charges are directly produced within the pulse duration. These charges are immediately relaxed by coupling with a phonon of the polythiophene (PT) backbone on femtosecond time scale

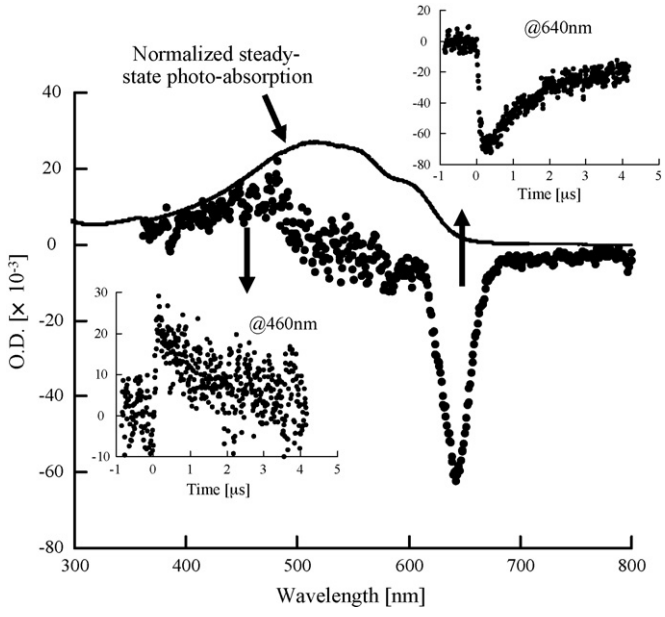

Fig. 3. Transient absorption spectra of RR-P3HT film induced by 193 nm laser. The insets show a kinetic traces at around 460 and 640 nm, which represent a photo absorption and a bleaching of ground state absorption, respectively.

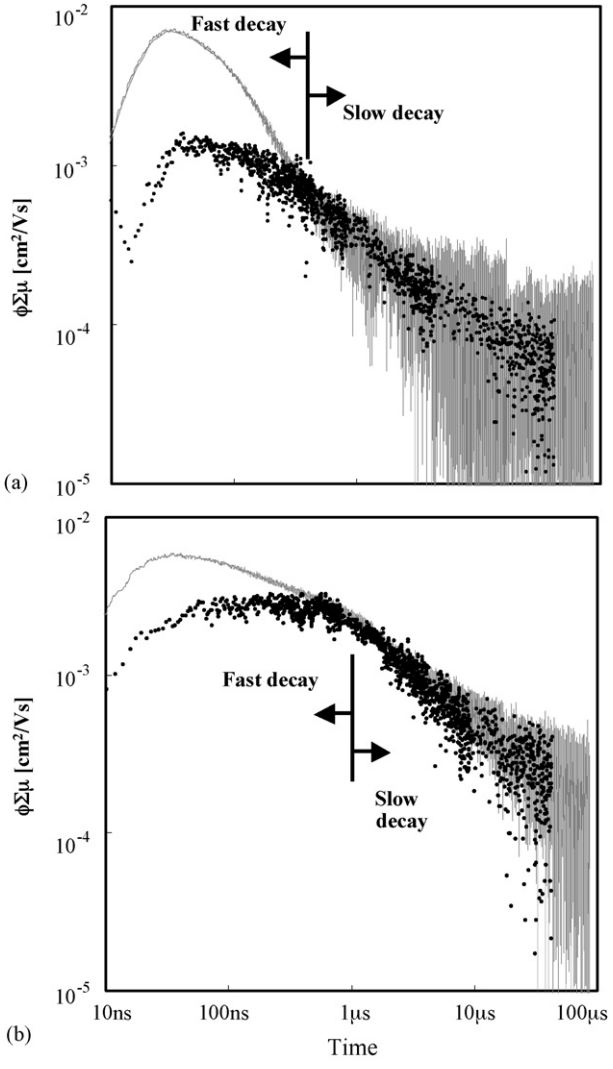

Fig. 4. TRMC (line) and TAS (closed circles) transients in RR-P3HT film excited by 193 nm laser. The TAS transients at 640 nm (bleaching) are inversely normalized to fit the kinetic traces of TRMC in long time region. The difference between (a) and (b) is the procedure of sample preparation (see text).

[18], giving rise to the positive and negative polarons (P^+, P^-):

$$PT \xrightarrow{h\nu} P^+ + P^-. \quad (10)$$

Using a charge carrier mobility reported in isolated molecule of polythiophene [9]: 0.014 $cm^2\ V^{-1}\ s^{-1}$, the quantum yield of charge carrier generation is calculated as >30%, suggesting the direct ionization of RR-P3HT molecules caused by193 nm exposure.

Both TRMC and TAS kinetic traces in Fig. 4(a) were obtained using the same sample which was prepared from a saturated *o*-dichlorobenzene solution of RR-P3HT. The solution was drop-casted on a quartz substrate and dried slowly at 80° in an oven. The lamellar structure would affect not only the mobility of charge carries but also the formation processes of charge carriers. The rise times of the TRMC and TAS signals in Fig. 4(a) are around 30 ns which corresponds to the dead time of a resonant cavity and the pulse duration of 193 nm laser. However, it should be noted that the decay kinetics of both TRMC and TAS in early time region up to ca. 400 ns differs considerably: the curve of TRMC decays rapidly while that of TAS decays slowly.

In general, a spectroscopy within a crystalline domain (lamellar structures) is difficult because of the scattering of a probe light. Therefore it is probable that the TAS probes only the transient species existing in amorphous regions. The fast decay in the kinetic trace of the TRMC would be due to the bulk recombination of positive and negative charges in the crystalline domains, because the TRMC can measure the averaged conductivity which comes from all charge carriers existing in both crystalline and amorphous domains:

$$P^+ + P^- \rightarrow S_1, T_1 \rightarrow S_0. \quad (11)$$

It should be emphasized that the charge carriers which possesses a large mobility are sensitized in TRMC signal because the amplitude of the signal is proportional to $\Sigma\mu$. This characteristic is compatible with the experimental observation that the kinetic traces of TRMC and TAS became identical after the fast decay of the TRMC transient completed at 400 ns. The 193 nm excitation generates directly charge carriers near the surface of a sample and the large part of TRMC signal comes from the area where the density of charge carriers is high. Therefore, the effect of domain boundaries on the formation process of charge carriers is expected to be small in the case of 193 nm excitation.

A slow decay of the TRMC signal after ca.400 ns is due to delayed charge recombination between trapped charge carriers at impurities or structural defects which essentially exist in polymeric materials:

$$P^+, P^- \rightarrow \text{trapped}. \quad (12)$$

In this delayed time region, the bulk recombination of charge carriers in crystalline domains would be completed. Consequently, the charge carrier in amorphous domains becomes predominant in which the charge carrier mobility is expected to be smaller than that in crystalline domains.

Fig. 4(b) also represents the TRMC and TAS signals, while the procedure of a sample preparation is different from Fig. 4(a). The film was prepared from a saturated methyl tetrahydrofuran solution of RR-P3HT. The solution was drop-casted on a quartz substrate and dried immediately at 50 °C in a vacuum oven. This procedure is expected to yield different film morphology from that in Fig. 4(a). Although the end-of-pulse value of $\phi\Sigma\mu$ in Fig. 4(b) is almost same as that in Fig. 4(a), the slope of the fast decay of TRMC signal decreases in Fig. 4(b). The difference between TRMC and TAS signals becomes small compared with that in Fig. 4(a). The amplitude of $\phi\Sigma\mu$ in the part of the slow decay becomes higher. These observations are consistent with the explanation described above: the fast and the slow decays are due to the bulk recombination in intra- and inter-crystalline domains and the delayed charge recombination affected by impurities or structural defects in amorphous regions, respectively. The degree of π-stacking in RR-P3HT was reported to vary depending on solvents, temperature of solvent evaporation, concentration of solutions, casting processes, and so on [19]. The decrease of the slope in the fast decay of TRMC signal would be caused by the change in the π-stacking structures and grain boundary, leading to the lower efficiency of intermolecular and inter-grain charge transfer. The increase of amplitude in the slow decay in Fig. 4(b) would be due to the increase of the amorphous regions.

The rise times of the TRMC and TAS signals in Fig. 4(b) are almost same as those in Fig. 4(a). The junction of the fast and slow decays in Fig. 4(b) was delayed to around 1 μs. The kinetic trace of TAS up to 1 μs was almost constant. This is suggestive that the charge carriers migrate to the amorphous regions and become detectable by the optical spectroscopy. The decay rates in the slow parts of the decay in both Fig. 4(a) and (b) are almost identical, suggesting that the properties in amorphous regions such as trapping rates are not affected by the solvent used for drop-casting.

In order to obtain information on the morphologies of the films, AFM observations were performed and are shown in Fig. 5. The micrographs of Fig. 5(a) and (b) represent the phase images of the film surface of Fig. 4(a) and (b), respectively. The images clearly demonstrate the different morphologies among the two samples, whereas the grains in Fig. 4(b), prepared from methyl tetrahydrofuran solution, are more inhomogeneous and more isolated than those in Fig. 4(a) prepared from *o*-dichlorobenzene.

It has been reported that the strong van der Waals interaction between the tip surface of an AFM probe and the lamellar surface of π-stacked P3HT causes considerable phase shift of the tapping resonance frequency of the probe, giving clear contrast of the lamellar and amorphous domains in the phase images of polythiophene thin films [20]. The domain size distribution was quantitatively analyzed based on the phase shift spectra (phase shift versus intensity obtained by a particle analysis of AFM measurement software) of the tapping probe observed for Fig. 5(a) and (b). By calculating the percentage of larger phase shift than that at the peaks of the spectra, the estimated relative ratios of the lamellar domains were 37 and 47%, respectively.

Fig. 5(c) represents the out-of-plane X-ray diffraction (XRD) patterns of both films, showing almost same widths and peaks. The strongest peak at ca. 5.4 Å is corresponds to the intermolecular spacing of 16.36 Å and consistent with literatures [21]. These

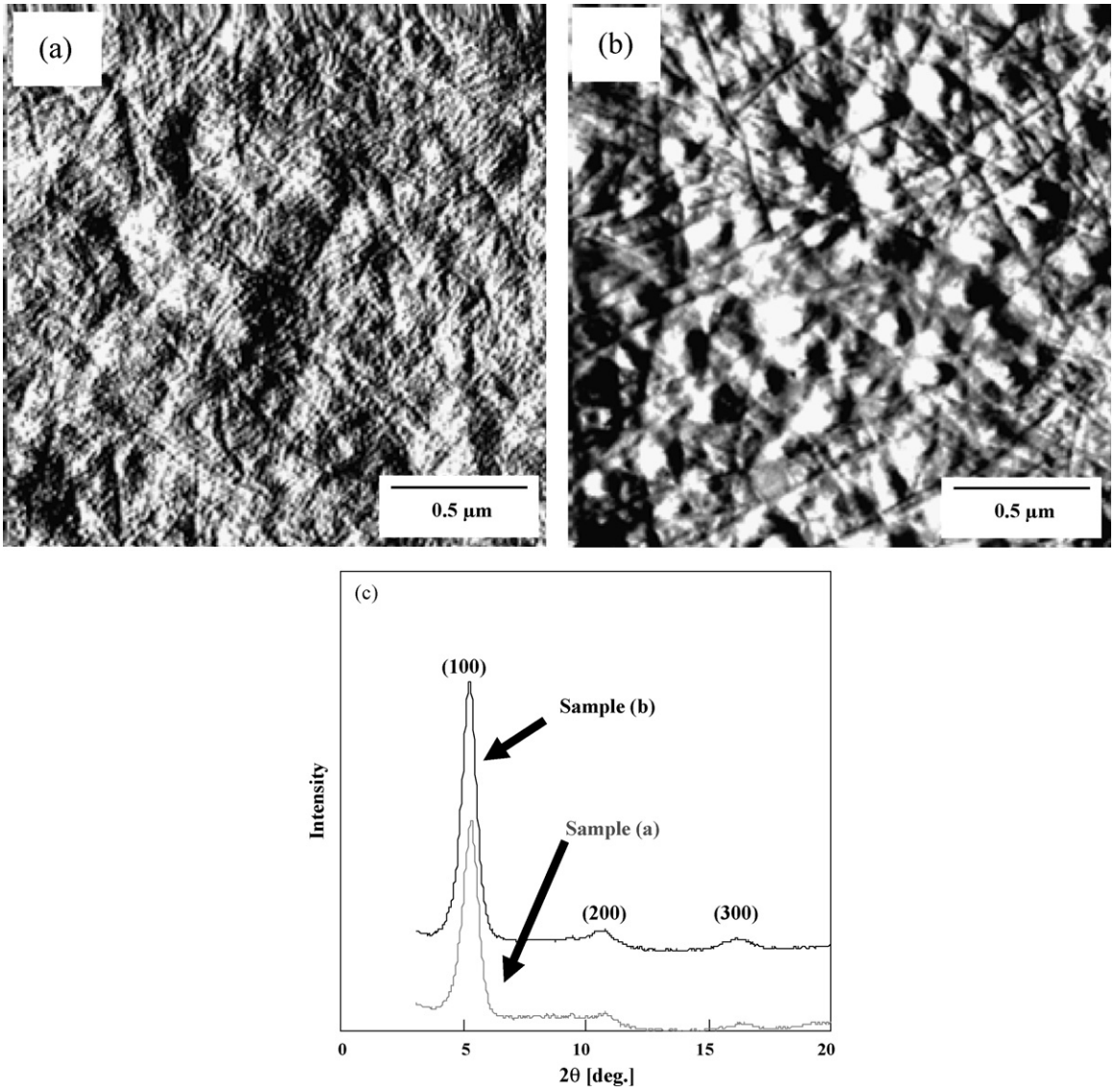

Fig. 5. Micrographs of RR-P3HT films. Images of (a) and (b) represent the phase images of the film samples of Fig. 4(a) and (b), respectively. (c) The out-of-plane XRD patterns of these films.

results suggest that although the lamellar structure induced by π-stacking is almost identical, the improved grain boundaries lower the barrier of inter-grain charge recombination, and thus, the fast TRMC decay is accelerated in the film of more homogeneously distributed grain. This scenario is consistent with the previous report describing detailed XRD analysis of RR-P3HT films [22], and analogous to the TRMC experiments in different grain size of pentacene films [23]. In addition, the surface morphology is predominant for the laser-induced conductivity, because the incident laser intensity exponentially decreases with the depth of the film (penetration depth, where the incident photon density decreases to $1/e$, was estimated as 91 nm using the steady-state absorption coefficient of $1.1 \times 10^7\ m^{-1}$ at 193 nm). Therefore, it is deduced that the fast decay observed in TRMC signal is due to the charge recombination inter- and intra-grain, while the slow decay is ascribed to the delayed charge recombination in amorphous region and charge trapping by impurities and structural defects.

Fig. 6 shows the TRMC and TAS signals in RR-P3HT induced by 355 nm laser of which photon energy is 3.5 eV. A film sample was prepared according to the same procedure as Fig. 4(a). The photon energy is much lower than the ionization potential of polythiophene, but higher than its band gap energy (∼2.1 eV) [24]. Therefore, the charge carrier generation via exciton dissociation is predominant. The fast decay was not observed, because a direct ionization is suppressed upon 355 nm exposure. The transient absorption spectrum is almost similar to that of 193 nm excitation, showing a broad absorption and sharp bleaching maxima at 460 and 640 nm, respectively. The kinetic traces at both maxima corresponds to each other, although the rise time of TAS signal was fast ca. 11 ns which reflects the pulse duration of Nd:YAG laser. On the other hand, TRMC signal indicates the rise time of 100–200 ns which is two to five times longer than the pulse duration and the response time of a resonant cavity. The slow rise time could be caused by the charge carrier generation from exciton dissociation in crystalline domains. According

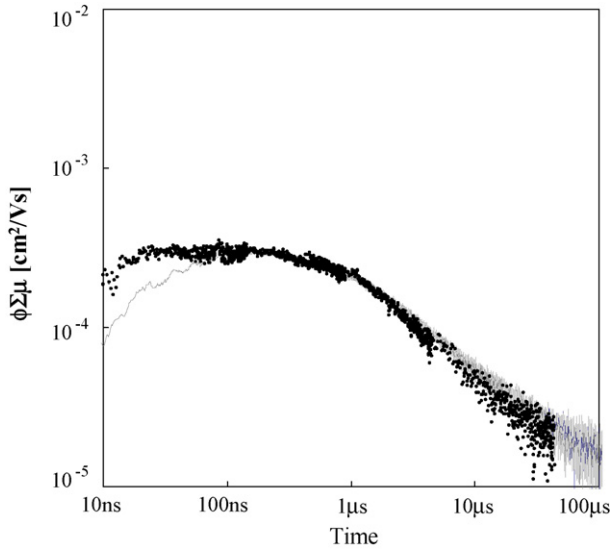

Fig. 6. TRMC (line) and TAS (closed circles) signals in RR-P3HT film excited by 355 nm laser. The TAS transient was observed at around 460 nm, which is symmetrically identical to the transient of the bleaching at 640 nm.

to Jiang et al. [5], ordered structure enhances the intermolecular interaction, giving a high yield of interchain exciton which dissociate more into polaron pairs. Dicker et al. [9]. also revealed that the vibrationally relaxed singlet exciton dissociation into charge carriers with a high yield in lamellar microstructure. This is the case giving the longer rise time in TRMC signals because of the delayed exciton dissociation at the boundary of the crystalline (lamellar) domains.

Upon laser exposure with photon energies below the ionization potential, there are several candidates of formation mechanisms of charge carriers such as multi-photon excitation, exciton–exciton annihilation, exciton dissociation assisted by thermal energy and/or electron acceptors, and so on. Based on the above discussions, the major path to give the positive charge carriers in the present case is represented as

$$\mathrm{PT} \xrightarrow{h\nu} \mathrm{S}_n \rightarrow \mathrm{S}_n, \mathrm{T}_n, \tag{13}$$

$$\mathrm{S}_n, \mathrm{T}_n + \mathrm{A} \rightarrow \mathrm{P}^+ + \mathrm{A}^-, \tag{14}$$

where A is the electron acceptors such as impurities and structure disordering in the bulk structures, S_n and T_n denote singlet exciton ($n \geq 1$) and triplet exciton ($n \geq 1$), respectively. It was reported from solution and solid-state studies that a rate constant of intersystem crossing is ca. 1 ns [25], the lifetime of a radiative singlet exciton is from a few hundreds of picoseconds [26] to a few tens of nanoseconds [27], and the lifetime of a triplet is ca. 20 μs [28,29]. According to the femtosecond photolysis studies [5], it was reported that long-lived triplet excitons are not easily generated in RR-P3HT lamellar and substantial intersystem crossing to the triplet occurs in regiorandom P3HT. While the rise time of TRMC signal was a few hundreds of nanoseconds in the present experiments on 355 nm exposure, the slow formation is expected to be to microsecond time scale, depending on the film conditions and electron acceptors. Thus we conclude that not only the singlet exciton but also the triplet exciton would play an important role in the delayed stage of photocarrier generation.

4. Conclusion

The transient conductivity and optical absorption induced by 193 and 355 nm laser in regioregular poly(3-hexylthiophene) was measured using in situ TRMC and TAS system on the time scale from 10 ns to 100 μs. The photon energy of 193 nm laser is sufficiently larger than the ionization potential of polythiophene, resulting in the high yield of photogeneration of charge carriers. The kinetic trace of TRMC signal excited by 193 nm laser consisted of two components: fast and slow decays. The former decay was not observed in 355 nm excitation of which photon energy is below the ionization potential but above the band gap of polythiophene.

On 193 nm excitation, the decay curve of TAS corresponded to that of TRMC in delayed time stage, while they did not in the early stage. The discrepancy would be due to the experimental difficulties in the spectroscopy of crystalline domains. The decay kinetics of both TRMC and TAS differed by changing the sample preparation which led to the change in the film morphology. From the XRD patterns and phase images observed by AFM, it is deduced that the fast decay observed in TRMC signal is due to the charge recombination inter- and intra-grain, while the slow decay is ascribed to the delayed charge recombination in amorphous region and charge trapping by impurities and structural defects.

The 355 nm excitation did not yield a fast decay as observed in 193 nm excitation. The rise time of TRMC was longer by a factor of 3–5 than dead time of resonant cavity. This is suggestive that not only the singlet exciton but also the triplet exciton would play an important role in the delayed stage of photocarrier generation.

Acknowledgments

We greatly appreciate the assistance of Dr. T. Kusunose at ISIR, Osaka University with XRD experiment. We would like to extend our gratitude to Mr. S. Tsukuda at ISIR, Osaka University for his assistance of AFM measurements. We also thank Mr. K. Abe at Canon Inc. for his assistance in experiments and meaningful discussion, and Dr. T. Sunagawa at Fukui University of Technology and Dr. K. Ushida at RIKEN, and Dr. A. Acharya at ISIR, Osaka University for their supports in the setup of TRMC experiments.

References

[1] T.A. Skotheim, R.L. Elsenbaumer, J.R. Reynolds (Eds.), Handbook of Conducting Polymer, Marcel Dekker, New York, 1998.
[2] H. Sirringhaus, P.J. Brown, R.H. Friend, M.M. Nielsen, K. Bechgaard, B.M.W. Langeveld-Voss, A.J.H. Spiering, R.A.J. Janssen, E.W. Meijer, P. Herwing, D.M. de Leeuw, Nature 401 (1999) 685.
[3] S. Seki, Y. Koizumi, T. Kawaguchi, H. Habara, S. Tagawa, J. Am. Chem. Soc. 126 (2004) 3521.
[4] L.S. Swanson, J. Shinar, K. Yoshino, Phys. Rev. Lett. 65 (1990) 1140.
[5] X.M. Jiang, R. Österbacka, O. Korovyanko, C.P. An, B. Horovitz, R.A.J. Janssen, Z.V. Vardeny, Adv. Funct. Mater. 12 (2002) 587.

[6] E.M. Conwell, H.A. Mizes, Phys. Rev. B 51 (1995) 6953.
[7] R.J.O.M. Hoofman, M.P. de Haas, L.D.A. Siebbeles, J.M. Warman, Nature 392 (1998) 54.
[8] F.C. Grozema, L.D.A. Siebbeles, J.M. Warman, S. Seki, S. Tagawa, U. Scherf, Adv. Mater. 14 (2002) 228.
[9] G. Dicker, M.P. de Haas, L.D.A. Siebbeles, J.M. Warman, Phys. Rev. B 70 (2004) 045203.
[10] A. Saeki, S. Seki, T. Sunagawa, K. Ushida, S. Tagawa, Philos. Mag. 86 (2006) 1261.
[11] A. Saeki, S. Seki, Y. Koizumi, T. Sunagawa, K. Ushida, S. Tagawa, J. Phys. Chem. B 109 (2005) 10015.
[12] P.P. Infelta, M.P. de Haas, J.M. Warman, Radiat. Phys. Chem. 10 (1977) 353.
[13] M.P. de Haas, J.M. Warman, Chem. Phys. 73 (1982) 35.
[14] J. Brandrup, E.H. Immergut, E.A. Grulke (Eds.), Polymer Handbook, 4th ed., John Wiley & Sons Inc., 2003.
[15] P.J. Brown, H. Sirringhaus, M. Harrison, M. Shkunov, R.H. Friend, Phys. Rev. B 63 (2001) 125204.
[16] P.J. Brown, D.S. Thomas, A. Köhler, J.S. Wilson, J.-S. Kim, C.M. Ramsdale, H. Sirringhaus, R.H. Friend, Phys. Rev. B 67 (2003) 064203.
[17] S. Morita, A.A. Zakhidov, T. Kawai, H. Araki, K. Yoshino, Jpn. J. Appl. Phys. 31 (1992) L890.
[18] E. Frankevich, H. Ishii, Y. Hamanaka, T. Yokoyama, A. Fujii, S. Li, K. Yoshino, A. Nakamura, K. Seki, Synth. Met. 119 (2001) 495.
[19] Z. Bao, A. Dodabalapur, A.J. Lovinger, Appl. Phys. Lett. 69 (1996) 4108.
[20] N. Zhao, G.A. Botton, S. Zhu, A. Duft, B.S. Ong, Y. Wu, P. Liu, Macromolecules 37 (2004) 8307.
[21] R.D. McCullough, S. Tristram-Nagle, S.P. Williams, R.D. Lowe, M. Jayaraman, J. Am. Chem. Soc. 115 (1993) 4910.
[22] R.J. Kline, M.D. Mcgehee, M.F. Toney, Nat. Mater. 5 (2006) 222.
[23] A. Saeki, S. Seki, S. Tagawa, J. Appl. Phys. 100 (2006) 023703.
[24] T.-C. Chung, J.H. Kaufman, A.J. Heeger, F. Wudl, Phys. Rev. B 30 (1984) 702.
[25] B. Kraabel, D. Moses, A.J. Heeger, J. Chem. Phys. 103 (1995) 5102.
[26] L. Magnani, G. Rumbles, I.D.W. Samuel, K. Murray, S.C. Moratti, A.B. Holmes, R.H. Friend, Synth. Met. 84 (1997) 899.
[27] G. Rumbles, I.D.W. Samuel, L. Magnani, K.A. Murray, A.J. DeMello, B. Crystall, S.C. Moratti, B.M. Stone, A.B. Holmes, R.H. Friend, Synth. Met. 76 (1996) 47.
[28] H.D. Burrows, J.S. de Melo, C. Serpa, L.G. Arnaut, M. da, G. Miguel, A.P. Monkman, I. Hamblett, S. Navaratnam, Chem. Phys. 285 (2002) 3.
[29] A.J. Cadby, P.A. Lane, D.D.C. Bradley, S.J. Holdcroft, C. Yang, Synth. Met. 119 (2001) 573.